Direct Dynamics Study of the Hydrogen-Abstraction Reaction of 1,1,2,2,3-Fluorinated Propane with the Hydroxyl Radical

Hong Gao, Ying Wang, Jing-yao Liu,* Lei Yang, Ze-sheng Li, and Chia-chung Sun

Institute of Theoretical Chemistry, State Key Laboratory of Theoretical and Computational Chemistry, Jilin University, Changchun 130023, People's Republic of China

Received: September 21, 2007; In Final Form: February 1, 2008

The hydrogen abstraction reactions by a hydroxyl radical from 1,1,2,2,3-fluorinated propane ($CF_2HCF_2CFH_2$) have been investigated by the dual-level direct dynamics method. Three equilibrium conformers (I, II, III) of $CF_2HCF_2CFH_2$, one with C_s and two with C_1 symmetries, are identified by the rotations of $-CFH_2$ and $-CF_2H$ groups. Two transition states are located for the conformer I (C_s symmetry) + OH → products (R1) reaction, and three distinct transition states are identified for conformers II and III (C_1 symmetry) + OH → products (R2 and R3). The optimized geometries and harmonic vibrational frequencies of all reactants, complexes, transition states, and products are calculated at the BB1K/6-31+G(d,p) level of theory. The single-point energy calculations are performed at the G3(MP2) level using the BB1K geometries. Using improved canonical variational transition-state theory (ICVT) with the small-curvature tunneling correction (SCT), the rate constants for each channel are calculated over a wide temperature range of 200−2000 K. It is found that the H-abstraction reaction from the $-CFH_2$ group is the predominant product channel for three reactions. The total rate constant is evaluated by the Boltzmann distribution function, and the agreement between theoretical and experimental values is good.

Introduction

Chlorofluorocarbons (CFCs) have been phased out because of their well-known depletion of the stratospheric ozone layer and the contribution to greenhouse effects. Therefore, many efforts have been made to search for alternatives to CFCs. Hydrofluorocarbons (HFCs), as an important class of potential CFC substitutes, are used in a wide range of industrial applications due to their zero ozone depletion potential value. However, they still have contributions to the global warming because of their high infrared absorbency and long atmospheric lifetimes. It is known that the reaction with the OH radical is the major tropospheric degradation process of the HFC, under both atmospheric and combustion conditions; thus, in order to assess its environmental impact and to estimate the atmospheric lifetime, the main removal process by OH has attracted considerable attention. In this work, the theoretical investigation was focused on the reaction of $CF_2HCF_2CFH_2$ + OH. Many experimental methods[1−3] have been applied to study the kinetics of this reaction. The authors reported the total rate constants and gave the Arrhenius expressions in lower temperature ranges of 286−364,[2] 260−365,[3] 200−300,[4] and 270−340[5] K. These Arrhenius expressions show good agreement. For this reaction, the hydrogen atoms are located in $-CF_2H$ and $-CFH_2$ sites, and thus, more than one reaction channel is possible. However, since it is difficult to determine which hydrogen can be abstracted in an experiment, no information on the mechanism or the branching ratios has been reported in their study. To provide a deep insight into the mechanisms and to understand the reaction dynamics of the title reaction, a high-level theoretical study is very desirable. Only Bartolotti[6] estimated the rate constant of this reaction at 298 K by the investigation of the correlation between the energy of the highest occupied molecular orbital (HOMO) and the logarithm of the OH rate constant of hydrofluorocarbons.

In the present study, we performed the dual-level direct dynamics method[7−9] to study the kinetic nature of the $CF_2HCF_2CFH_2$ + OH reaction over the temperature range of 200−2000 K. In this approach, the required electronic structure information for the stationary points and a series of extra points along the minimum energy path (MEP) were obtained directly from ab initio or density functional theory (DFT) calculations. Subsequently, by means of the POLYRATE 8.4.1 program,[10] the rate constants were determined using the variational transition-state theory (VTST)[11−13] proposed by Truhlar and co-workers for each reaction channel, and a description of the temperature dependence is given. Since three low-energy conformers of $CF_2HCF_2CFH_2$, one with C_s and two with C_1 symmetries, are located by the rotations of the $-CF_2H$ and $-CFH_2$ groups, the relative population of three conformers are considered in the overall rate constant calculation. Our present study is relevant to the understanding of the tropospheric chemistry of $CF_2HCF_2CFH_2$.

Calculation Methods

BB1K (Becke88[14]−Becke95[15] one-parameter model for kinetics methods)[16] is a new metahybrid density functional theory method developed by Truhlar et al. It has been demonstrated that the BB1K method with the 6-31+G(d,p) basis set is very powerful and accurate in the potential energy surface (PES) calculation. Therefore, in this study, the electronic structure calculations including the equilibrium geometries and frequencies of the stationary points involved in the reactions (R1, R2, and R3) are performed at the BB1K/6-31+G(d,p) level. The minimum-energy path (MEP) is calculated by the intrinsic

* To whom correspondence should be addressed. Fax: +86-431-88498026. E-mail: ljy121@jlu.edu.cn.

10.1021/jp077611z CCC: $40.75
Published on Web 04/03/2008

reaction coordinate (IRC) theory at the same level to confirm that the TS really connects with minima along the reaction path. Also, first and second energy derivatives at geometries along the MEP are obtained to calculate the curvature of the reaction path and to calculate the generalized vibrational frequencies along the reaction path. To gain more reliable energy information, single-point energy calculations for the stationary points are carried out at the G3(MP2)[17]level using the BB1K-optimized geometries. The energy profiles are refined with the interpolated single-point energies (ISPE) method[18] at the G3(MP2)//BB1K/6-31+G(d,p) level. In the present study, single-point energies evaluated at four nonstationary points (ISPE-4) are used to improve the lower-level reaction path. The Gaussian 03 program packages[19] are employed to carry out all of the electronic structure calculations.

The initial information of the potential energy profile is put into the POLYRATE 8.4.1 program to evaluate the rate constants. The rate constants are calculated by using the variational transition-state theory (VTST) proposed by Truhlar and co-workers. The specific level of VTST that we used is improved canonical variational transition-state theory (ICVT).[20] The transmission coefficient is calculated by the centrifugal-dominant small-curvature semiclassical adiabatic ground-state tunneling (SCT),[21,22] which has been successfully used in the study for many H-abstraction reactions.[23−25] It should be noted that for a reaction including the transfer of a light particle between two heavy atoms, the large-curvature tunneling (LCT) probability may be important, especially at low temperature, while the LCT method requires more information of the potential energy surface (PES) and not just the MEP, which is beyond the scope of our work. Because the harmonic frequencies for the internal rotation in the transition states are found to be low, the hindered rotor model is used to consider the lowest vibrational mode, and the other vibrational modes are treated as separable harmonic oscillators. In the calculation of the electronic partition functions, two electronic states for OH radicals, with a 140 cm^{-1} splitting in the $^2\Pi$ ground state, are included.

Results and Discussion

1. Stationary Points. Two equilibrium conformers (I and II) of the $CF_2HCF_2CFH_2$ with C_s and C_1 symmetries are characterized by the rotation of the $-CFH_2$ group, and the calculated potential energy profile connecting the two conformers is shown in Figure 1a. The C_s conformer is found to be slightly lower in energy. In order not to lose other stable conformers, the $-CF_2H$ group is rotated under the C_s and C_1 symmetry configuration. The energy profiles as a function of twist angle C−C−C−F (F in the $-CF_2H$ site) based on conformers I and II are plotted in Figures b and c, respectively. In Figure 1b, two other stable structures with almost the same energy are found along the potential energy profile, but they have not been taken into consideration because their energies are higher by about 2.24 kcal mol^{-1} than that of the conformer I at the BB1K/6-31+G(d,p) level. Similarly, the two other stable conformers are identified in Figure 1c; the one which has the lowest energy is denoted as conformer III, and the other with higher energy by about 2.05 kcal mol^{-1} than that of conformer II is also beyond our consideration. Conformer III is found to be the most stable conformer, of which the energy is less than that of conformer I and II by about 0.52 and 0.74 kcal mol^{-1}, respectively, at the BB1K/6-31+G(d,p) level, and the energy differences amount to 0.50 and 0.76 kcal mol^{-1} at the G3(MP2) level of theory, respectively. These small energy differences

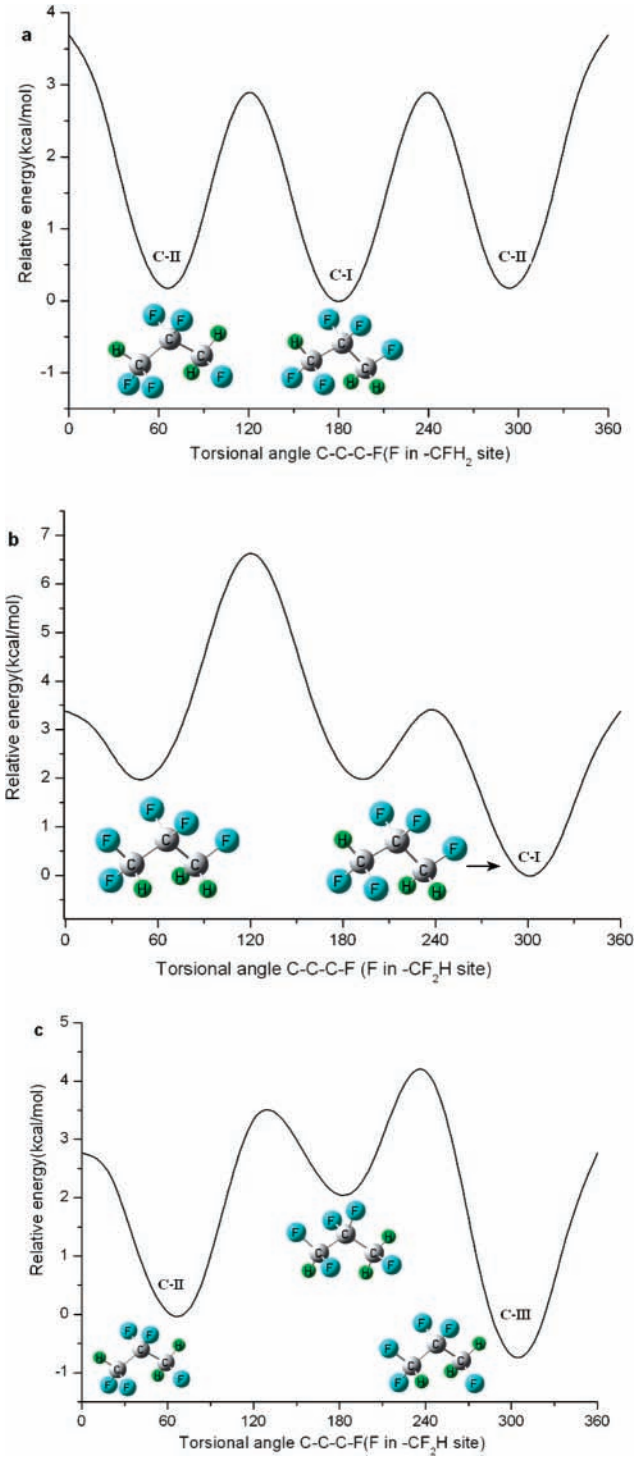

Figure 1. Torsional potential function for $CF_2HCF_2CFH_2$ calculated from the BB1K/6-31+G(d,p) results. The relative energies for conformer I are shown in Figure 1a,b, and similarly, the relative energies for conformer II are shown in Figure 1c.

provide evidence that the conformers will contribute to the title reaction by the weight factors estimated from the Boltzmann distribution. As for the reactant with C_s symmetry, the hydrogen atoms in the $-CFH_2$ site are equivalent; therefore, two H-abstraction channels, one from $-CF_2H$ and the other from $-CFH_2$ group, are feasible, denoted as R1a and R1b

$$CF_2HCF_2CFH_2\ (C_s) + OH \rightarrow CF_2CF_2CFH_2 + H_2O \quad \text{(R1a)}$$

$$\rightarrow CF_2HCF_2CFH + H_2O \quad \text{(R1b)}$$

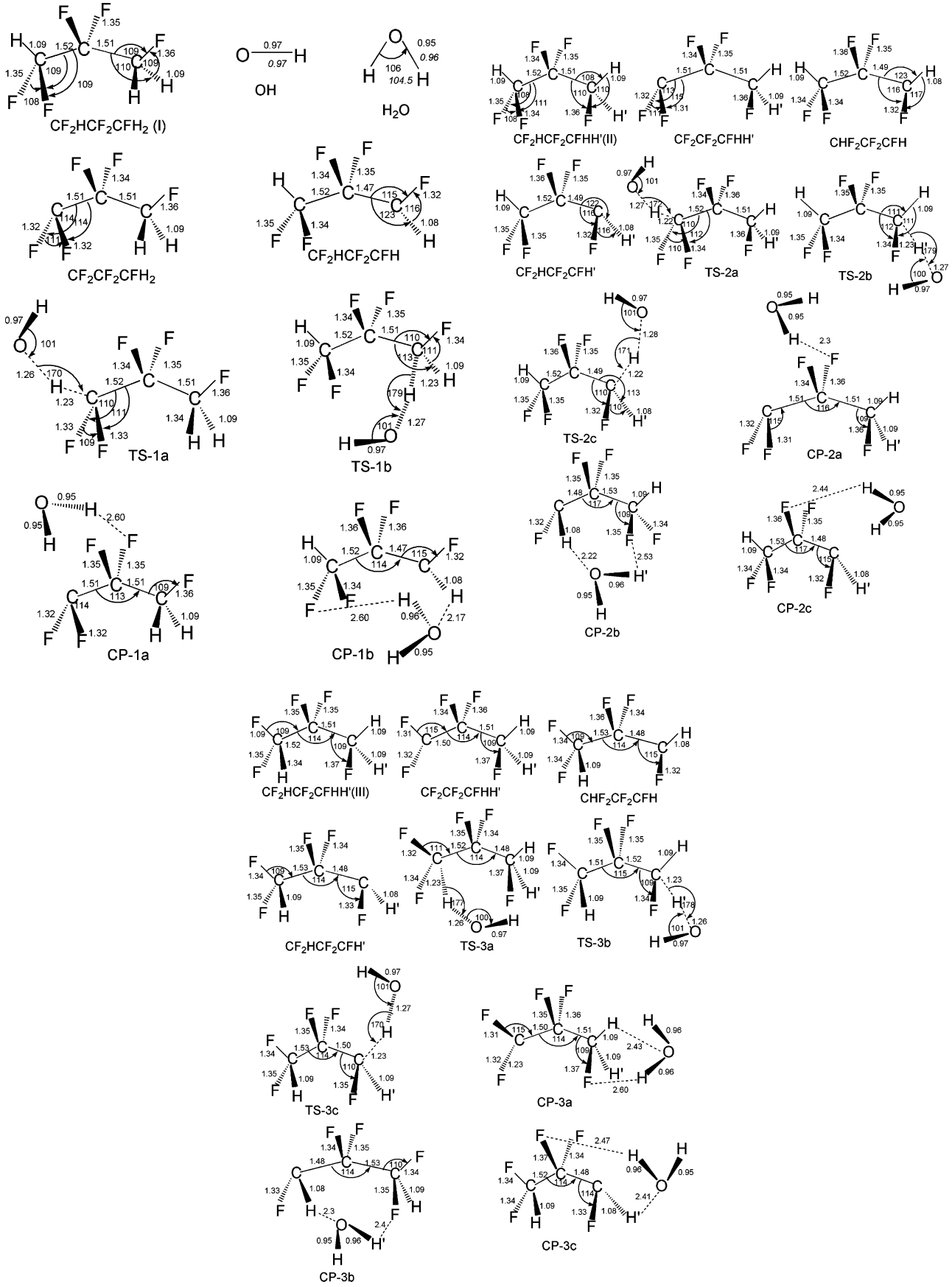

Figure 2. Optimized geometries parameters (in Å and deg) of the reactants, complexes, products, and transition states (TSs) at the BB1K/6-31+G(d,p) level, as well as the available experimental values.[26] The experimental values are given in italic.

Because none of the hydrogen atoms in the two conformers with C_1 symmetry are equivalent, these distinguished channels are found according to the different position. These channels are denoted as follows

$$CF_2HCF_2CFHH'\ (C_1) + OH \rightarrow CF_2CF_2CFHH' + H_2O \quad \text{(R2a and R3a)}$$

$$\rightarrow CF_2HCF_2CFH + HOH' \quad \text{(R2b and R3b)}$$

$$\rightarrow CF_2HCF_2CFH' + H_2O \quad \text{(R2c and R3c)}$$

The geometric parameters of all of the stationary points involved in reactions R1, R2, and R3 optimized at the BB1K/6-31+G(d,p) level are shown in Figure 2, as well as the available experimental values.[26] Because of the high electronegativity of the fluorine atom and the oxygen atom, hydrogen bonds are formed between F and H atoms as well as between H and O atoms. Therefore, the hydrogen-bonded complexes with energies less than those of the products are located at the exit channels of reactions R1, R2, and R3, which means that the reactions may proceed via an indirect mechanism. In the complexes, the hydrogen-bond lengths of O···H and H···F are all less than the sum of their van der Waals radii (2.72 and 2.67 Å), and the other bond lengths are very close to those of the products. For example, in complex CP1b, the bond distances of O···H and H···F are 2.17 and 2.60 Å, respectively, less than the sum of their van der Waals radii. In addition, in the transition-state structures of eight hydrogen-abstraction channels, that is, TS-1a, TS-1b, TS-2a, TS-2b, TS-2c, TS-3a, TS-3b, and TS-3c, the breaking C−H bonds are elongated by 13, 13, 12, 13, 12, 13, 13, and 13%, respectively, compared to the C−H regular bond lengths in the isolated reactants at the BB1K level, and the forming H−O bonds are stretched by 33, 34, 34, 34, 35, 31, 31, and 32%, respectively, with respect to the equilibrium bond lengths of the molecule H_2O. The elongation of the forming bond is greater than that of the breaking bond, indicating that these transition states are reactant-like, that is, these eight reaction channels proceed via "early" transition states. This early character in the TSs is in keeping with Hammond's postulate[27] for exothermic reactions.

The reaction enthalpies (ΔH^{o}_{298}) calculated at the BB1K/6-31+G(d,p) and the G3(MP2)//BB1K/6-31+G(d,p) levels are listed in Table 1. From Table 1, we can see that the all of the reaction channels are exothermic, and the reaction channels of R2 are more exoergic than the corresponding channels of R1and R3. The ΔH^{o}_{298} values at the G3(MP2) level are −13.47 and −16.09 kcal mol^{-1} for R1a and b, −14.55, −16.08, and −16.41 kcal mol^{-1} for R2a−c, and −14.07, −15.25, and −15.30 kcal mol^{-1} for R3a−c, respectively.

The harmonic vibrational frequencies are calculated at the same level of theory to characterize the nature of each critical point and to make zero-point energy (ZPE) corrections. Table 2 lists the harmonic vibrational frequencies of all of the stationary points along with the available experimental values[28] of OH and H_2O. As can be seen, the agreement between the calculated and experimental ones is good, with the maximum error within 8.9%. The number of imaginary frequencies (0 or 1) indicates whether a minimum or a transition state has been located. All of the reactants and products have only real frequencies. The transition state is confirmed by normal-mode analysis to have only one imaginary frequency, which takes the values of 1584i, 1540i, 1490i, 1563i, 1429i, 1610i, 1590i and 1515i cm^{-1} for TS-1a, TS-1b,TS-2a, TS-2b, TS-2c, TS-3a, TS-3b, and TS-3c, respectively. These larger absolute values of imaginary frequency indicate that the width of the potential barrier might be narrower and the tunneling effect may be important in the calculation of the rate constant.

A schematic potential energy profiles of reactions R1−R3 obtained at the G3(MP2)//BB1K/6-31+G(d,p) level with zero-point energy (ZPE) correction are plotted in Figure 3a−c. The energy of the reactant is set to zero for reference. Each reaction passes through a reactant-like transition state to form a product complex, which is at a lower energy than that of the corresponding products. The energy of TS-1a, 5.28 kcal mol^{-1}, is slightly lower than that of TS-1b by 0.15 kcal mol^{-1}. However, it should be toted that in the present study, a dual-level (B//A) method, that is, energy corrected at higher level B using the geometries at lower level A, is used to reproduce the features of the reaction path. As pointed out by Espinosa-Garcia and Corchado,[29] using the B//A technique to construct the MEP could cause a shift of the energy maximum at the B level with respect to the maximum at the A level. Thus, if we compared the maximum of the single-point calculation curves of R1a and R1b, we can find that R1b has an actual lower barrier than that of R1a (6.01 vs 5.95 kcal mol^{-1}). Also, reaction path R1b is more exothermic than the former by 2.78 kcal mol^{-1}. Thus, the reaction pathway R1b is both kinetically and thermodynamically more favorable than pathway R1a.

TABLE 1: Enthalpies (kcal mol^{-1}) at 298 K at the BB1K/6-31+G(d,p) and G3(MP2)//BB1K Levels

reaction		levels	ΔH^{o}_{298}
$CF_2HCF_2CFH_2$(I) + OH →		BB1K	−11.86
$CF_2CF_2CFH_2 + H_2O$	(R1a)	G3(MP2)	−13.47
		BB1K	−14.14
$CF_2HCF_2CHF + H_2O$	(R1b)	G3(MP2)	−16.09
CF_2HCF_2CFHH'(II) + OH →		BB1K	−13.11
$CF_2CF_2CFHH' + H_2O$	(R2a)	G3(MP2)	−14.55
		BB1K	−14.00
$CF_2HCF_2CFH + HOH$	(R2b)	G3(MP2)	−16.08
		BB1K	−14.34
$CF_2HCF_2CFH' + H_2O$	(R2c)	G3(MP2)	−16.41
CF_2HCF_2CFH'(III) + OH →		BB1K	−12.68
$CF_2CF_2CFHH' + H_2O$	(R3a)	G3(MP2)	−14.07
		BB1K	−13.18
$CF_2HCF_2CFH + HOH$	(R3b)	G3(MP2)	−15.25
		BB1K	−13.20
$CF_2HCF_2CFH' + H_2O$	(R3c)	G3(MP2)	−15.30

For the reaction channels of R2, the barrier heights are 4.88, 5.04, and 4.71 kcal mol^{-1} and the exothermic values are −14.78, −16.51, and −16.73 kcal mol^{-1}, respectively. It is seen that R2c is the most exoergic and has the lowest barrier height; therefore, reaction path R2c will be most likely the dominant channel. For the comparison of channels R2a and R2b, a similar case as that for R1a and R1b is found. Although the barrier height of R2a is slightly lower than that of R2b by about 0.16 kcal mol^{-1}, the maximum of the energy curve of R2a obtained at a higher level is slightly larger than the corresponding value of R2b, and the exothermic values of R2a are less than that of R2b by about 1.73 kcal mol^{-1}. Therefore, R2a may be less competitive than R2b. For reaction R3, channel R3a is kinetically more favorable due to the lowest barrier height, while both R3b and R3c are thermodynamically more feasible. Also, from Figure 3c, it is seen that the barrier height of R3b is less than that of R3c by about 0.1 kcal mol^{-1}. Therefore, from the view of energetics of these three channels, we predict that channels R3a and R3b may be more competitive than R3c.

2. Rate Constant Calculations. The minimum-energy path (MEP) is calculated by the intrinsic reaction coordinate (IRC) theory at the BB1K/6-31+G(d,p) level from the transition state to the reactant and product, and the potential energy profile is further refined with ISPE method at the G3(MP2)//BB1K level. The classical potential energy curves ($V_{MEP}(s)$), the vibrationally adiabatic ground-state potential energy curves ($V_a^G(s)$), and the zero-point energy (ZPE(s)) curves of the R1b, R3a, and R3b channels as a function of the intrinsic reaction coordinate(s)

TABLE 2: Calculated Frequencies (cm^{-1}) of the Stationary Points at the BB1K/6-31+G(d,p) Level, along with the Experimental Values (Experimental Values Given in the Parentheses)

species	frequencies (cm^{-1})	species	frequencies (cm^{-1})
OH	3859 (*3735*[a])	CP-2a	9,24,58,82,87,111,135,197,240,249,287,361, 413,490,535,577,678,820,992,1155,1184, 1204,1266,1315,1351,1437,1470,1524,1640, 3159,3233,3962,4084
H_2O	1636, 3963, 4089 (*1595, 3657, 3756*[a])	CP-2b	26,53,82,96,113,138,173,211,219,268,307, 358,411,485,546,576,646,722,877,1160, 1189,1218,1221,1255,1310,1401,1423,1499, 1655,3198,3303,3960,4084
$CF_2HCF_2CFH_2$(I)	67,80,156,200,276,347,360,516,538,602,709, 832,993,1163,1179,1193,1226,1258,1299, 1334,1402,1467,1478,1524,3166,3208,3236	CP-2c	36,54,67,97,138,148,198,240,272,334,360, 413,426,505,569,588,624,701,876,1166,1196, 1214,1227,1259,1294,1403,1419,1497,1671, 3199,3331,3973,4094
$CF_2CF_2CFH_2$	58,96,157,203,272,352,360,519,535,628,674, 832,1002,1114,1171,1239,1284,1328,1359, 1420,1476,1521,3156,3225	CP-3a	40,56,71,123,135,174,196,219,249,347,406, 478,489,549,575,598,707,808,982,1146,1154, 1198,1297,1319,1349,1461,1479,1524,1658, 3177,3256,3957,4076
CHF_2CF_2CFH	59,72,154,198,280,315,359,471,541,591,612, 716,867,1136,1179,1202,1242,1269,1305, 1403,1463,1505,3211,3324	CP-3b	32,62,68,98,110,135,183,206,229,252,363, 410,482,495,554,603,639,761,876,1132,1174, 1212,1221,1284,1298,1404,1450,1473,1657, 3210,3307,3958,4079
CF_2HCF_2CFHH(II)	46,111,181,203,264,358,406,484,543,571,669, 856,1007,1165,1179,1206,1215,1250,1313, 1353,1406,1448,1498,1523,3159,3198,3230	CP-3c	37,48,67,82,109,124,168,185,232,256,331, 415,468,476,541,593,664,707,871,1104,1188, 1208,1218,1256,1321,1405,1468,1469,1651, 3211,3325,3956,4078
CF_2CF_2CFHH'	54,125,186,212,280,359,409,487,537,577,677, 821,993,1153,1186,1217,1264,1314,1344, 1436,1468,1526, 3158,3232	TS-1a	1584i,54,84,95,122,161,169,206,283,350, 361,428,516,554,626,740,823,924,997,1162, 1172,1189,1228,1277,1301,1339,1366,1471, 1495,1522,3161,3232,3874,
CF_2HCF_2CFH	42,118,197,225,228,358,379,416,492,573,592, 697,887,1154,1189,1207,1221,1266,1320, 1406,1427,1503,3200, 3322,	TS-2b	1540i,32,80,124,136,169,186,212,281,340, 362,512,535,586,647,708,787,886,1025,1177, 1193,1208,1213,1259,1301,1309,1402,1424, 1470,1495,3210,3216,3892
CF_2HCF_2CFH'	49,119,192,223,269,358,412,451,506,570,629, 706,876,1170,1195,1219,1223,1261,1300, 1402,1421,1497,3198,3319	TS-2a	1490i,46,94,110,129,161,188,242,267,360, 406,431,519,537,603,701,799,927,1017,1163, 1178,1194,1221,1282,1294,1322,1401,1450, 1483,1511,3160,3234,3877
CF_2HCF_2CFH'(III)	62,102,179,231,252,345,408,477,551,612,693, 869,981,1148,1181,1207,1215,1272,1302, 1332,1414,1467,1482,1530,3169,3215,3242	TS-2b	1563i,31,83,125,155,194,207,212,295,357, 407,449,535,568,651,672,806,906,1073,1148, 1175,1202,1228,1229,1258,1344,1405,1408, 1464,1494,3159,3201,3890
CF_2CF_2CFHH'	54,96,173,215,241,341,408,476,571,598,700, 805,978,1146,1163,1201,1278,1323,1350, 1460,1468,1527,3164,3235	TS-2c	1429i,41,71,80,138,175,196,239,265,359, 408,494,542,570,666,725,818,887,1050,1167, 1188,1201,1215,1231,1276,1312,1407,1426, 1467,1472,3196,3213,3880
CHF_2CF_2CFH	51,90,172,226,241,302,404,471,510,573,637, 713,872,1134,1189,1217,1223,1252,1329, 1412,1468,1480,3204,3317	TS-3a	1610i,47,96,121,136,180,217,241,254,334, 406,422,497,564,623,714,786,958,990,1142, 1166,1201,1233,1274,1286,1323,1396,1464, 1482,1521,3174,3249,3884
CF_2HCF_2CFH'	59,80,164,225,251,332,406,465,526,580,611, 746,873,1137,1187,1216,1228,1273,1307, 1409,1453,1473,3205,3324	TS-3b	1590i,44,61,88,113,179,191,237,260,333, 410,473,539,594,632,730,795,872,1069,1145, 1174,1189,1214,1241,1267,1308,1400,1428, 1468,1493,3208,3220,3889
CP-1a	45,68,78,100,122,128,160,208,276,355,360, 472,519,539,613,631,674,831,1000,1116, 1170,1232,1282,1326,1357,1420,1479,1522, 1656,3157,3227,3966,4089	TS-3c	1515i,55,70,104,134,170,214,235,258,317, 405,477,556,604,688,724,849,892,1039,1146, 1187,1191,1215,1232,1284,1317,1412,1430, 1467,1478,3216,3222,3885
CP-1b	26,65,83,97,122,134,164,195,214,290,355, 371,411,543,551,609,671,717,870,1138,1166, 1196,1225,1268,1315,1402,1465,1520,1662, 3210,3302,3964,4085		

[a] From ref 28.

are plotted in Figure 4a−c, where $V_a^G(s)$ is obtained by summing $V_{MEP}(s)$ and ZPE(s). As seen from Figure 4a, the maximum of the potential energy profile at the G3(MP2)//BB1K/6-31+G-(d,p) level is slightly shifted in the s direction. This is the case in which the saddle point position of the dual level is generally shifted with the VTST-ISPE scheme, which indicates that the variational effect may play a role in the rate constant calculation for R1b. Similar behavior can be drawn from reactions R1a, R2a, R2c, and R3c. Figure S1 is given for the four channels as Supporting Information. In Figure 4b,c, it is found that the V_{MEP} and V_a^G curves are similar in shape, and the ZPE is practically constant as s varies, with only a gentle drop near the saddle point, which means that the variational effect is very small or almost negligible for reaction R3a and R3b. Similarly, the R2b channel also has the same nature and is shown in Figure S1 as Supporting Information.

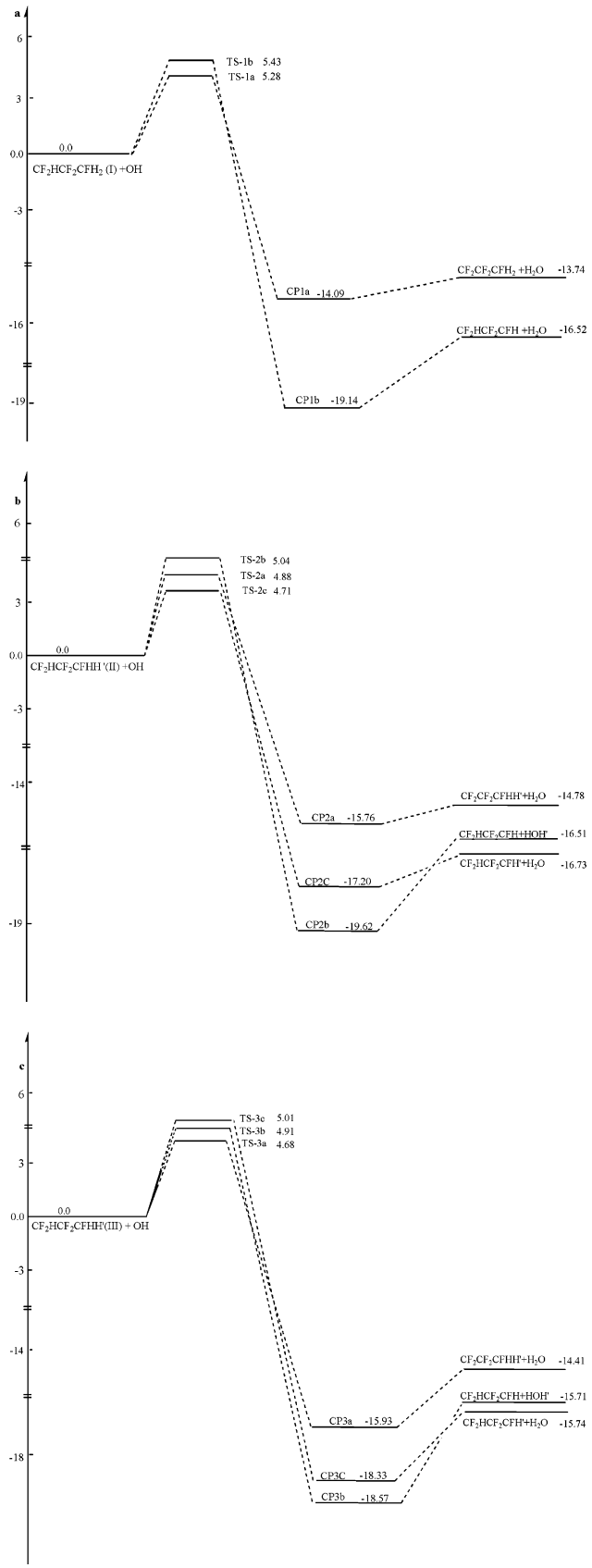

Figure 3. Schematic pathways (a) for the reaction $CF_2HCF_2CFH_2(I) + OH \rightarrow$ products, (b) for the reaction $CF_2HCF_2CFHH'(II) + OH \rightarrow$ products, and (c) for the reaction $CF_2HCF_2CFHH'(III) + OH \rightarrow$ products. Relative energies with ZPE correction at the G3(MP2)//BB1K/6-31+G(d,p) level are in kcal mol^{-1}.

Dual-level (X//Y) direct dynamics calculations are carried out for reactions R1, R2, and R3. The PES information for each reaction obtained at the G3(MP2)//BB1K/6-31+G(d,p) level is put into the POLYRATE 8.4.1 program to calculate the VTST rate constants over the temperature range from 200 to 2000 K.

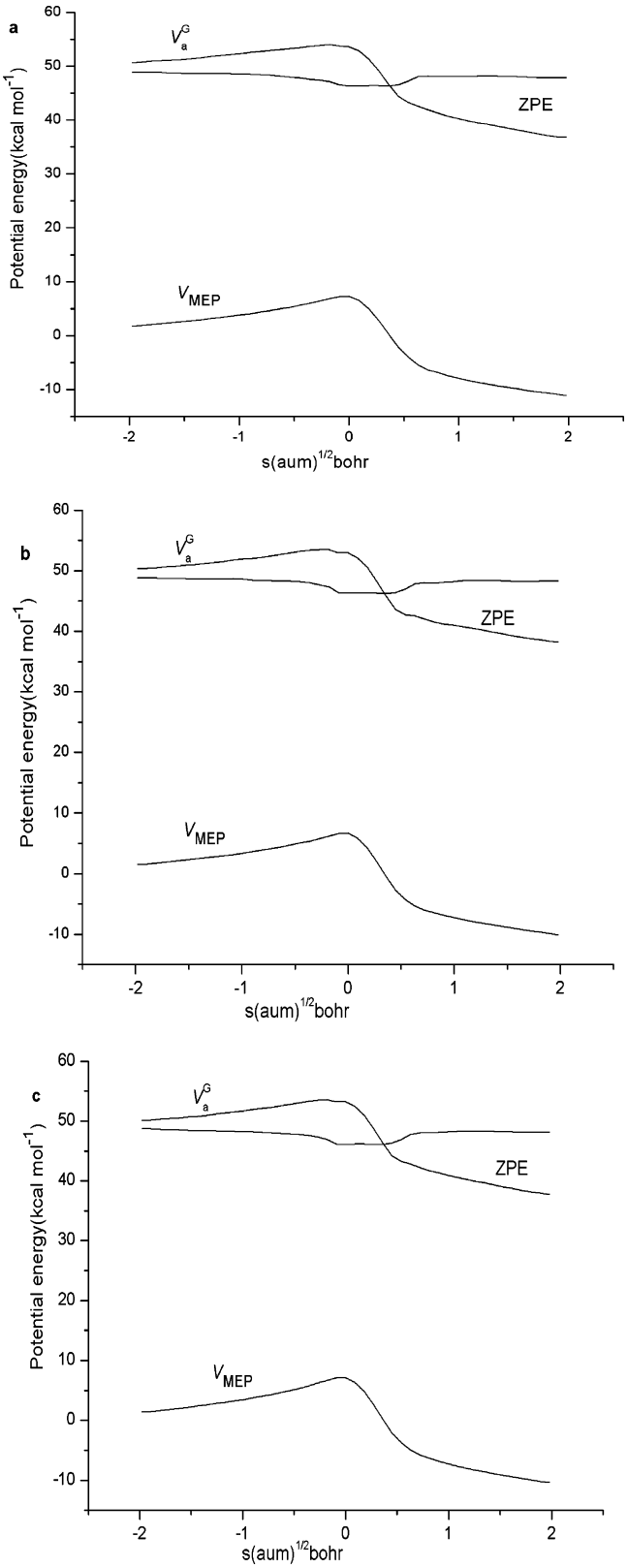

Figure 4. Classical potential energy curve (V_{MEP}), ground-state vibrationally adiabatic energy curve (V_a^G), and zero-point energy curve (ZPE) as functions of s (amu)$^{1/2}$ bohr at the G3(MP2)level (a) for the reaction $CF_2HCF_2CFH_2(I) + OH \rightarrow CF_2HCF_2CFH + H_2O$ (R1b), (b) for the reaction $CF_2HCF_2CFHH'(III) + OH \rightarrow CF_2CF_2CFHH' + H_2O$ (R3a), and (c) for the reaction $CF_2HCF_2CFHH'(III) + OH \rightarrow CF_2HCF_2CFH + HOH'$ (R3b).

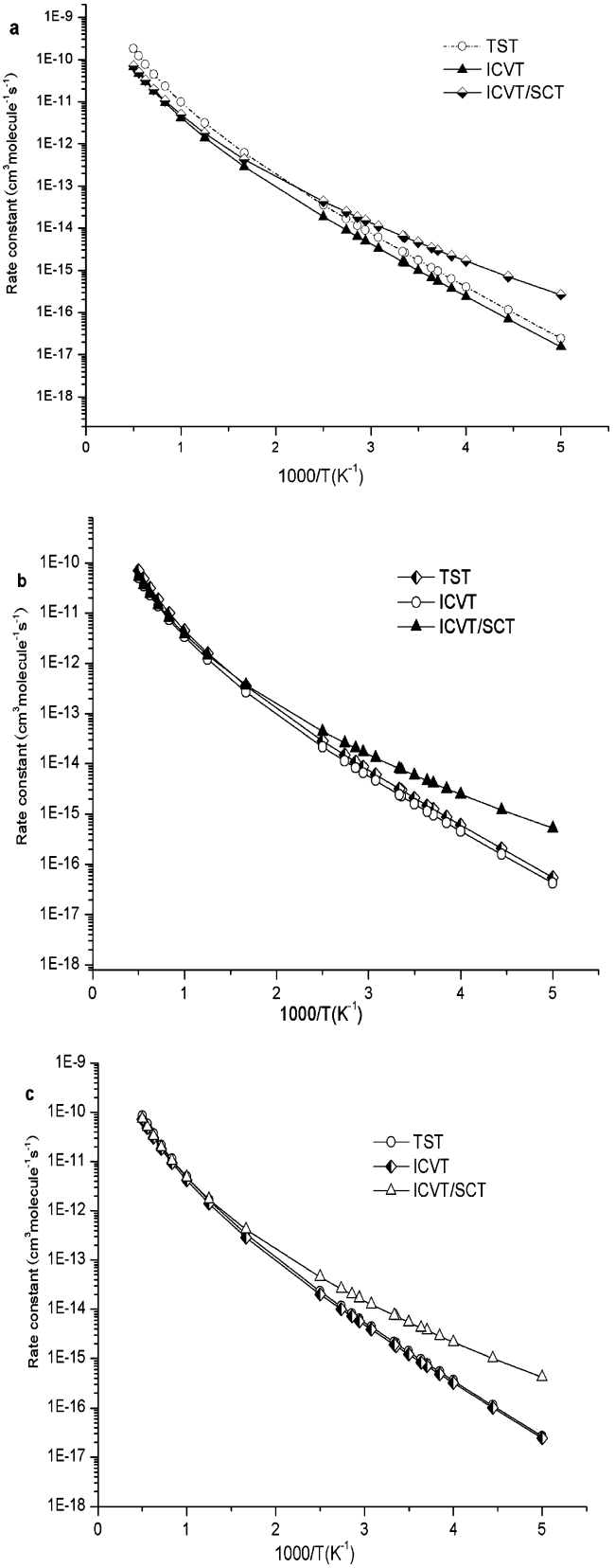

Figure 5. Plots of TST, ICVT, and ICVT/SCT rate constants calculated at the G3 (MP2)//BB1K/6-31+G(d,p) level versus 1000/*T* between 200 and 2000 K (a) for the reaction $CF_2HCF_2CFH_2(I) + OH \rightarrow CF_2HCF_2CFH + H_2O$ (R1b), (b) for the reaction $CF_2HCF_2CFHH'(III) + OH \rightarrow CF_2CF_2CFHH' + H_2O$ (R3a), and (c) for the reaction $CF_2HCF_2CFHH'(III) + OH \rightarrow CF_2HCF_2CFH + HOH'$ (R3b).

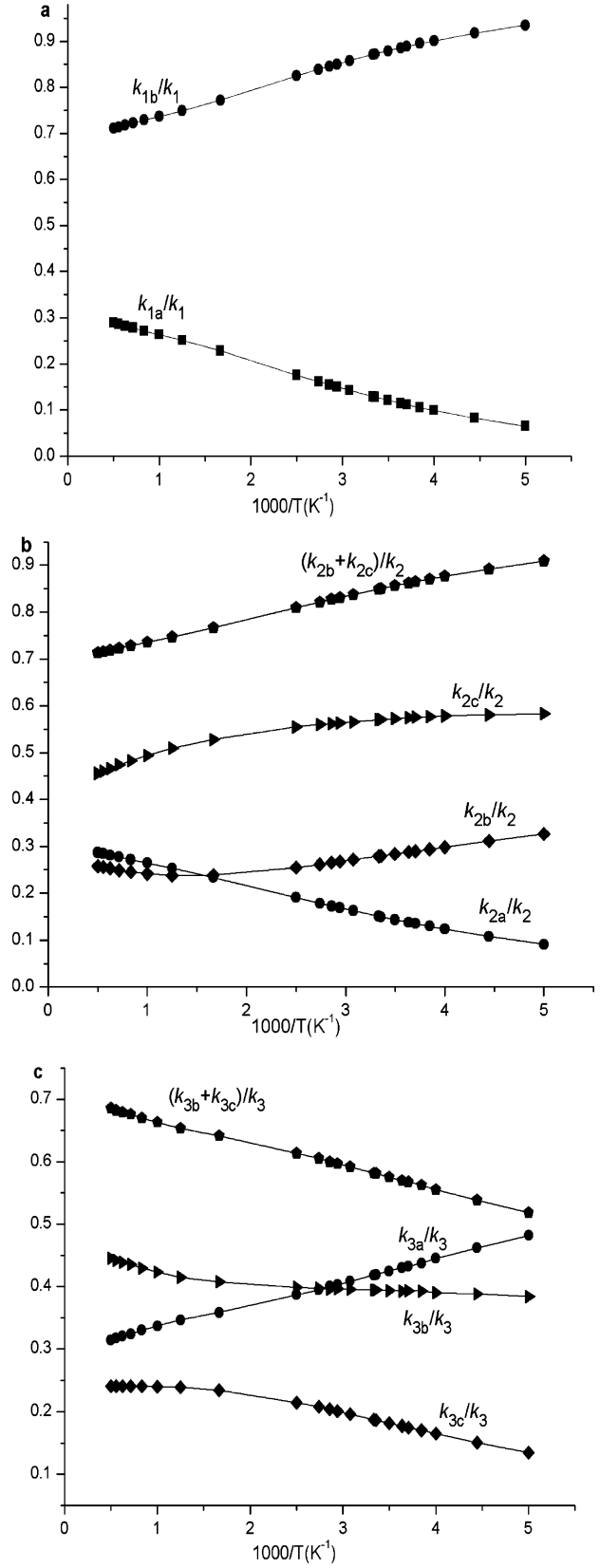

Figure 6. Plots of the calculated branching ratios versus 1000/*T* between 200 and 2000 K (a) for the reaction $CF_2HCF_2CFH_2(I) + OH \rightarrow$ products, (b) for the reaction $CF_2HCF_2CFHH'(II) + OH \rightarrow$ products, and (c) for the reaction $CF_2HCF_2CFHH'(III) + OH \rightarrow$ products.

The forward rate constants are calculated by conventional transition-state theory (TST), the improved canonical variational transition-state theory (ICVT), and ICVT with the small-curvature tunneling (SCT) correction.

The TST, ICVT, and ICVT/SCT rate constants of channels R1b, R3a, and R3b are presented in Figure 5 a−c, respectively,

TABLE 3: Calculated ICVT/SCT Rate Constants (in cm³ molecule⁻¹ s⁻¹) for the Reactions $CF_2HCF_2CFH_2$(I) + OH → Products (R1), CF_2HCF_2CFHH'(II) + OH → Products (R2), and CF_2HCF_2CFHH'(III) + OH → Products (R3) as Well as the Experimental Values in the Temperature Range of 200−2000 K at the G3(MP2)//BB1K/6-31+G(d,p) Level of Theory

T(K)	k_1	k_2	k_3	k_T	exptl
200	2.83×10^{-16}	1.71×10^{-16}	1.08×10^{-15}	8.30×10^{-16}	5.98×10^{-16} [d]
225	7.74×10^{-16}	4.84×10^{-16}	2.59×10^{-15}	1.94×10^{-15}	1.5×10^{-15} [d]
250	1.83×10^{-15}	1.17×10^{-15}	5.50×10^{-15}	4.05×10^{-15}	3.15×10^{-15} [d]
260	2.50×10^{-15}	1.62×10^{-15}	7.24×10^{-15}	5.31×10^{-15}	4.85×10^{-15} [c]
270	3.35×10^{-15}	2.19×10^{-15}	9.37×10^{-15}	6.85×10^{-15}	4.0×10^{-15} [e]
275	3.86×10^{-15}	2.52×10^{-15}	1.06×10^{-14}	7.76×10^{-15}	6.87×10^{-15} [c]; 5.76×10^{-15} [d]; 4.48×10^{-15} [e]
286	5.19×10^{-15}	3.42×10^{-15}	1.38×10^{-14}	1.01×10^{-14}	6.06×10^{-15} [b]
298	7.03×10^{-15}	4.68×10^{-15}	1.82×10^{-14}	1.32×10^{-14}	6.5×10^{-15} [a]; 6.7×10^{-15} [a]
300	7.38×10^{-15}	4.91×10^{-15}	1.90×10^{-14}	1.38×10^{-14}	7.94×10^{-15} [b]; 1.14×10^{-14} [c]; 9.52×10^{-15} [d]; 7.48×10^{-15} [e]
325	1.31×10^{-14}	8.84×10^{-15}	3.19×10^{-14}	2.29×10^{-14}	1.22×10^{-14} [b]; 1.74×10^{-14} [c]; 1.15×10^{-14} [e]
340	1.79×10^{-14}	1.22×10^{-14}	4.23×10^{-14}	3.04×10^{-14}	1.45×10^{-14} [e]
350	2.18×10^{-14}	1.49×10^{-14}	5.06×10^{-14}	3.63×10^{-14}	1.75×10^{-14} [b]; 2.5×10^{-14} [c]
365	2.89×10^{-14}	1.98×10^{-14}	6.54×10^{-14}	4.69×10^{-14}	3.04×10^{-14} [c]
400	5.23×10^{-14}	3.62×10^{-14}	1.13×10^{-13}	8.08×10^{-14}	
600	5.53×10^{-13}	3.88×10^{-13}	1.03×10^{-12}	7.30×10^{-13}	
800	2.38×10^{-12}	1.64×10^{-12}	4.14×10^{-12}	2.93×10^{-12}	
1000	6.65×10^{-12}	4.50×10^{-12}	1.12×10^{-11}	7.92×10^{-12}	
1200	1.45×10^{-11}	9.67×10^{-12}	2.42×10^{-11}	1.69×10^{-11}	
1600	4.47×10^{-11}	2.94×10^{-11}	7.43×10^{-11}	5.13×10^{-11}	
2000	9.89×10^{-11}	6.45×10^{-11}	1.65×10^{-10}	1.13×10^{-10}	

[a] From ref 1. [b] From ref 2. [c] From ref 3. [d] From ref 4. [e] From ref 5.

and the related data and the SCT tunneling corrections are listed in Table S1 as Supporting Information. Because two H atoms in the $-CFH_2$ site of the conformer I (C_s symmetry) are considered and the second site (in the $-CF_2H$ site) only has one hydrogen atom, the symmetry factors $\sigma = 1$ and 2 are considered in the rate constant calculations of R1a and R1b, respectively, that is to say, R1b has a statistical advantage. It can be seen that in the reaction channel for R1b, the TST values are larger than ICVT at the lower temperature range, which indicates that the variational effect plays a role in the rate constants. For example, the ratios of k_{ICVT}/k_{TST} are 0.63 and 0.56 at 200 and 298 K, respectively. Similar conclusion can be drawn for R1a, R2a, R2c, and R3c, and the corresponding plots are given in Figure S2 as Supporting Information. As shown in Figure 5b,c, the TST and ICVT rate constants of reactions R3a and R3b are nearly the same or almost negligible over the whole temperature range, which means that the variational effect is very small. Similarly, the R2b also has the same nature, and the plot is depicted in Figure S2 as Supporting Information. On the other hand, by contrasting the ICVT and ICVT/SCT values, we find that the SCT correction should be taken into account in the rate constant calculations for all channels at low temperature, while as the temperature increases, it is almost negligible. For example, the ratios of $k_{ICVT/SCT}/k_{ICVT}$ are 17.21, 12.37, and 17.05 at 200 K, and 1.16, 1.12, and 1.15 at 1000 K for R1b, R3a, and R3b, respectively.

The temperature dependence of the branching ratios of R1, R2, and R3 is exhibited in Figure 6 a−c. Figure 6a shows that k_{1a}/k_1 is small or negligible, and a H atom is abstracted almost exclusively from the $-CFH_2$ site, that is, R1b is the predominant channel for reaction R1 over the whole temperature range. For the reaction of conformer II + OH, reaction path R2c is the most feasible channel, consistent with the analysis above. The values of k_{2c}/k_2 are 0.58 and 0.46 at 200 and 2000K, respectively. In the low-temperature range, the contribution of channel R2b to the total rate constant is more important than that of R2a; for example, the ratios of k_{2a}/k_2 and k_{2b}/k_2 are 0.09 and 0.33 at 200 K. However, as the temperature increases, channel R2a become comparable to R2b; the corresponding ratios are 0.19 and 0.25 at 400 K and 0.26 and 0.24 at 1000 K, respectively. For the reaction of conformer III + OH, we can see that R3a is a more important channel than R3b at low temperature; for example, the values of k_{3a}/k_3 and k_{3b}/k_3 are 0.48 and 0.38 at 200 K. However, as the temperature increases, R3b becomes more and more important, and the values of k_{3a}/k_3 and k_{3b}/k_3 are 0.39 and 0.40 at 400 K and 0.34 and 0.42 at 1000 K, respectively, while R3c is the least over the whole temperature range. Moreover, in all cases, considering the fact that two hydrogen atoms in the $-CFH_2$ site are indistinguishable in the experimental observation, we can conclude that H abstractions from the $-CFH_2$ site (i.e., $k_{nb} + k_{nc}$, $n = 2, 3$) in the three conformers of $CF_2HCF_2CFH_2$ are the major reaction channels based on our calculation (as shown in Figure 6b,c).

The overall rate constant for reactions R1, R2 and R3 are obtained from the sum of the individual ICVT/SCT results associated with the available reaction paths ($k_1 = k_{1a} + k_{1b}$, $k_2 = k_{2a} + k_{2b} + k_{2c}$, and $k_3 = k_{3a} + k_{3b} + k_{3c}$). Then, the total rate constant (k_T) for the title reaction of $CF_2HCF_2CFH_2$ + OH → products can be obtained from the following expression

$$k_T = \omega_1 k_1 + \omega_2 k_2 + \omega_3 k_3$$
$$= \omega_1(k_{1a} + k_{1b}) + \omega_2(k_{2a} + k_{2b} + k_{2c}) + \omega_3(k_{3a} + k_{3b} + k_{3c})$$
$$= k_{1T} + k_{2T} + k_{3T} \quad \text{(E1)}$$

where ω_1, ω_2, and ω_3 are the weight factors of each conformer calculated from the Boltzmann distribution function. The temperature dependence of the ICVT/SCT rate constants of each reaction and the total rate constant are presented in Table 3 and Figure 7, along with the corresponding experimental values.[1−5] From them, we can find that the theoretical rate constants are in reasonable agreement with the available experimental value, with the maximum deviation within a factor of 2, and the rate constant (1.3×10^{-14} cm³ molecule⁻¹ s⁻¹) at 298 K is slightly less than the one evaluated by Bartolotti[6] (2.0×10^{-14} cm³ molecule⁻¹ s⁻¹). In addition, from expression E1, it is easy to evaluate what degree of each conformer contributes to the total rate constant. For example, the ω_1, ω_2, and ω_3 are 0.20, 0.10,

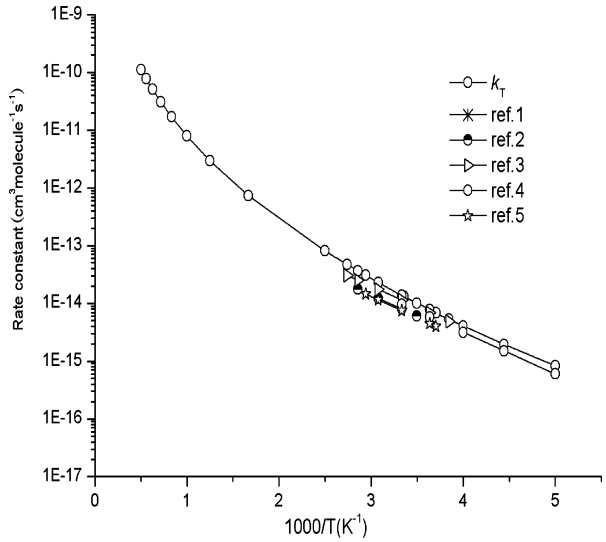

Figure 7. Plot of the rate constant k calculated by Boltzmann distribution function and the available experimental values[1−5] versus 1000/T between 200 and 2000K for the H-abstraction reaction of 1,1,2,2,3-fluorinated propane with the OH radical.

and 0.70 at 200 K and 0.33, 0.30, and 0.37 at 2000 K, respectively. The $k_{3T/kT}$ changes from 0.91 to 0.54 within 200−2000 K, which indicates that hydrogen abstraction from the conformer III dominates the reaction over the whole temperature range.

Also, the Arrhenius expression $k = 3.70 \times 10^{-12} \exp(-1692/T)$ (cm^3 molecule^{-1} s^{-1}) fitted by the ICVT/SCT rate constants in the 200−300 K temperature range agrees well with the expression $k = 2.41 \times 10^{-12} \exp(-1660 \pm 149/T)$ (cm^3 molecule^{-1} s^{-1}) reported by DeMore et al.[4] Since there is few data available at other temperatures, for providing theoretical prediction for the title reaction, the three-parameter fit for k_1, k_2, k_3, and k_T within 200−2000 K is given as follows (in cm^3 molecule^{-1} s^{-1})

$$k_1 = 6.03 \times 10^{-21} T^{3.19} \exp(-1238.10/T)$$

$$k_2 = 1.40 \times 10^{-20} T^{3.02} \exp(-1334.57/T)$$

$$k_3 = 2.08 \times 10^{-21} T^{3.38} \exp(-959.96/T)$$

$$k_T = 1.35 \times 10^{-21} T^{3.38} \exp(-937.45/T)$$

Conclusion

In this paper, the mechanisms of the hydrogen-abstraction reaction of rotamer 1,1,2,2,3-fluorinated propane (conformers I, II, and III) with the hydroxyl radical are investigated theoretically. The PES information is obtained by a new meta density functional theory method BB1K and at the G3(MP2) (single-point energy) level of theory. The rate constant calculations are carried out using the improved canonical variational transition-state theory (ICVT) with the small-curvature tunneling correction (SCT) at the G3(MP2)//BB1K/6-31+G(d,p) level over a wide temperature range of 200−2000 K. It is shown that the variational effect and SCT should be taken into account in the rate constant calculations. The theoretical rate constants agree well with the available experimental values, with the maximum deviation within a factor of 2, and the temperature dependence of the overall rate constant is fitted by a three-parameter expression within 200−2000 K. The present calculation suggests that conformer III dominates the title reaction over the whole temperature range. We hope that the theoretical results may be useful for estimating the kinetics of the reaction over a wide temperature range where no experimental data are available.

Acknowledgment. We thank Professor Donald G. Truhlar for providing the POLYRATE8.4.1 program. This work was supported by the National Natural Science Foundation of China (20303007, 20333050, and 20073014), the Doctor Foundation of the Ministry of Education, the Foundation for University Key Teacher of the Ministry of Education, the Key Subject of Science and Technology of the Ministry of Education of China, and the Key Subject of Science and Technology of the Jilin Province. The authors are grateful to the referees for their valuable comments on improving the manuscript.

Supporting Information Available: Additional energy curves and rate constant plots and tables. This material is available free of charge via the Internet at http://pubs.acs.org.

References and Notes

(1) Urata, S.; Takada, A.; Uchimaru, T.; Chandra, A. K. *Chem. Phys. Lett.* **2003**, *368*, 215.

(2) Hsu, K.-J.; DeMore, W. B. *J. Phys. Chem.* **1995**, *99*, 1235.

(3) Zhang, Z.; Padmaja, S.; Saini, R. D.; Huie, R. E.; Kurylo, M. J. *J. Phys. Chem.* **1994**, *98*, 4312.

(4) DeMore, W. B.; Sander, S. P.; Golden, D. M.; Hampson, R. F.; Kurylo, M. J.; Howard, C. J.; Ravishankara, A. R.; Kolb, C. E.; Molina, M.J. *JPL Publication 97-4*; Jet Propulsion Laboratory, California Institute of Technology: Pasadena, CA, 1997; Vol. 12.

(5) Atkinson, R.; Baulch, D. L.; Cox, R. A.; Hampson, R. F., Jr.; Kerr, J. A.; Rossi, M. J.; Troe, J. *J. Phys. Chem. Ref. Data* **1997**, *26*, 521.

(6) Bartolotti, L. J. *Int. J. Chem. Kinet.* **1994**, *26*, 913.

(7) Truhlar, D. G. *Direct Dynamics Method for the Calculation of Reaction Rates*. In *The Reaction Path in Chemistry: Current Approaches and Perspectives*; Heidrich, D., Ed.; Kluwer: Dordrecht, The Netherlands, 1995; p 229.

(8) Truhlar, D. G.; Garrent, B. C.; Klippenstein, S. J. *J Phys Chem.* **1996**, *100*, 12771.

(9) Hu, W. P.; Truhlar, D. G. *J. Am. Chem. Soc.* **1996**, *118*, 860.

(10) Chuang, Y. Y.; Corchado, J. C.; Fast, P. L.; Villa, J.; Hu, W. P.; Liu, Y. P.; Lynch, G. C.; Jackels, C. F.; Nguyen, K. A.; Gu, M. Z.; Rossi, I.; Coitino, E. L.; Clayton, S.; Melissas, V. S.; Lynch, B. J.; Steckler, R.; Garrett, B. C.; Isaacson, A. D.; Truhlar, D. G. *POLYRATE*, v. 8.4.1; University of Minnesota: Minneapolis, MN, 2000.

(11) Truhlar, D. G.; Garrett, B. C. *Acc. Chem. Res.* **1980**, *13*, 440.

(12) Truhlar, D. G.; Isaacson, A. D.; Garrett, B. C. *The Theory of Chemical Reaction Dynamics*; Baer, M., Ed.; CRC Press: Boca Raton, FL, 1985; p 65.

(13) Truhlar, D. G.; Garrett, B. C. *Annu. Rev. Phys. Chem.* **1984**, *35*, 159.

(14) Becke, A. D. *Phys. Rev. A* **1988**, *38*, 3098.

(15) Becke, A. D. *J. Chem. Phys.* **1996**, *104*, 1040.

(16) Zhao, Y.; Lynch, B. J.; Truhlar, D. G. *J. Phys. Chem. A* **2004**, *108*, 2715.

(17) Curtiss, L. A.; Redfern, P. C.; Raghavachari, K.; Rassolov, V.; Pople, J. A. *J. Chem. Phys.* **1999**, *110*, 4703.

(18) Chuang, Y. Y.; Corchado, J. C.; Truhlar, D. G. *J. Phys. Chem. A* **1999**, *103*, 1140.

(19) Frisch, M. J.; Truck, G. W.; Schlegel, H. B.; Scuseria, G. E.; Robb, M. A.; Cheeseman, J. R.; Zakrzewski, V. G.; Montgomery, J. A., Jr.; Stratmann, R. E.; Burant, J. C.; Dapprich, S.; Millam, J. M.; Daniels, A. D.; Kudin, K. N.; Strain, M. C.; Farkas, O.; Tomasi, J.; Barone, V.; Cossi, M.; Cammi, R.; Mennucci, B.; Pomelli, C.; Adamo, C.; Clifford, S.; Ochterski, J.; Petersson, G. A.; Ayala, P. Y.; Cui, Q.; Morokuma, K.; Malick, D. K.; Rabuck, A. D.; Raghavachari, K.; Foresman, J. B.; Cioslowski, J.; Ortiz, J. V.; Boboul, A. G.; Stefnov, B. B.; Liu, G.; Liaschenko, A.; Piskorz, P.; Komaromi, L.; Gomperts, R.; Martin, R. L.; Fox, D. J.; Keith, T.; Al-Laham, M. A.; Peng, C.Y.; Nanayakkara, A.; Gonzalez, C.; Challacombe, M.; Gill, P. M. W.; Johnson, B.; Chen, W.; Wong, M. W.; Andres, J. L.; Gonzalez, C.; Head-Gordon, M.; Replogle E. S.; Pople, J. A. *Gaussian 03*, revision A.1; Guassian, Inc.: Pittsburgh, PA, 2003.

(20) Garrett, B. C.; Truhlar, D. G.; Grev, R. S.; Magnuson, A. W. *J. Phys. Chem.* **1980**, *84*, 1730.

(21) Lu, D. H.; Truong, T. N.; Melissas, V. S.; Lynch, G. C.; Liu, Y. P.; Grarrett, B. C.; Steckler, R.; Issacson, A. D.; Rai, S. N.; Hancock, G. C.; Lauderdale, J. G.; Joseph, T.; Truhlar, D. G. *Comput. Phys. Commun.* **1992**, *71*, 235.

(22) Liu, Y.-P.; Lynch, G. C.; Truong, T. N.; Lu, D.-h.; Truhlar, D. G.; Garrett, B. C. *J. Am. Chem. Soc.* **1993**, *115*, 2408.

(23) Taghikhani, M.; Parsafar, G. A.; Sabzyan, H. *J. Phys. Chem. A* **2005**, *109*, 8158.

(24) Galano, A.; Alvarez-ldaboy, J. R.; Ruiz-Santoyo, M. E.; Vivier-Bunge, A. *Chem. Phys. Chem* **2004**, *5*, 1379.

(25) Wang, Y.; Liu, J.; Li, Z.; Wang, L.; Wu, J.; Sun, C. *J. Phys. Chem. A* **2006**, *110*, 5853.

(26) Lide, D. R. *CRC Handbook of Chemistry and Physics*, 80th ed.; CRC Press: New York, 1999.

(27) Hammond, G. S. *J. Am. Chem. Soc.* **1955**, *77*, 334.

(28) Shimanouchi, T. *Tables of Molecular Vibrational Frequencies Consolidated*; National Bureau of Standards; U. S. Government Printing Office: Washinton, DC, 1972; Vol. 1.

(29) Espinosa-Garcia, J.; Corchado, J. C. *J. Phys. Chem.* **1995**, *99*, 8613.